

Electronic Origin of Ferromagnetic Excitations in the Candidate Spin-Triplet Superconductor CeSb₂

Xiaoxiao Wang,^{1,2} Xiaoyang Chen,² Suppanut Sangphet,² Yifei Fang,³ Yilin Wang,^{4,5} Chihao Li,² Minyinan Lei,² Nan Guo,² Yuanhe Song,² Rui Peng,^{1,2,*} Haichao Xu,^{1,2,†} and Donglai Feng⁵

¹Shanghai Research Center for Quantum Sciences, Shanghai 201315, China

²Laboratory of Advanced Materials, State Key Laboratory of Surface Physics, and Department of Physics, Fudan University, Shanghai 200438, China

³State Key Laboratory of Ultra-intense Laser Science and Technology,

Shanghai Institute of Optics and Fine Mechanics, Chinese Academy of Sciences, 201800 Shanghai, China

⁴School of Emerging Technology, University of Science and Technology of China, Hefei 230026, China.

⁵New Cornerstone Science Laboratory, Hefei National Laboratory, Hefei, 230026, China

(Dated: May 29, 2026)

The origin of quasi-one-dimensional (q1D) ferromagnetic (FM) excitations in the candidate spin-triplet superconductor CeSb₂ has remained unclear. Here we report an electronic mechanism for emergent q1D magnetism in the quasi-two-dimensional lattice of CeSb₂, revealed by angle-resolved photoemission spectroscopy (ARPES). High-resolution ARPES resolves no spin-density-wave gap on the dispersive Fermi pockets, disfavoring a nesting-driven mechanism for the q1D FM excitations. Instead, resonant ARPES reveals a pronounced selective enhancement of Ce *4f* spectral weight on the *C*₂-distributed Fermi pockets aligned with the Ce ladder. This observation signifies band-selective Kondo coupling that generates strongly anisotropic magnetic exchange interactions, which can naturally account for both the q1D ferromagnetic excitations and the competing magnetic orders. Our results identify a band-selective Kondo coupling mechanism for emergent low-dimensional magnetism in correlated *f*-electron systems.

Unconventional superconductivity is widely believed to arise from pairing mechanisms involving magnetic fluctuations rather than conventional electron-phonon coupling [1–4]. For spin-triplet superconductivity, a phase of broad interest both for its fundamental novelty and for its potential relevance to topological quantum computing [5–14], ferromagnetic (FM) fluctuations have long been considered a critical ingredient for spin-triplet pairings. FM fluctuations have been observed in many candidate materials including K₂Cr₃As₃ and UTe₂ [5, 8, 9, 11, 15–19]. Identifying the interactions between such FM fluctuations and low-energy electronic states in candidate materials is therefore central to understanding spin-triplet pairing.

CeSb₂ has recently been identified as a candidate for pressure-induced spin-triplet superconductivity [20, 21]. INS measurements on CeSb₂ resolve well-defined quasi-one-dimensional (q1D) FM excitations that persist well above the magnetic ordering temperature, offering a possible FM channel relevant for triplet pairing [21]. However, the microscopic origin of these q1D FM excitations is unclear. CeSb₂ crystallizes in a quasi-two-dimensional (q2D) lattice with nearly identical inter- and intra-ladder Ce-Ce distances [Fig. 1(a)], so the lattice geometry cannot explain the dimensional reduction of the magnetic response. Moreover, the system does not condense into simple FM order but goes through four successive magnetic transitions below $T \sim 16$ K [22–24], including a commensurate AFM order with propagation vectors $(-1, \pm\frac{1}{6}, 0)$ [21, 25]. Together, the q1D FM excitations in a near-isotropic q2D lattice and the multiple magnetic orders raise the possibility that the effective dimensionality of the magnetic interactions is determined not by the lattice geometry itself. This calls for a microscopic mechanism rooted in the

electronic structure.

Here, we address this issue by directly probing the electronic structure of CeSb₂ using angle-resolved photoemission spectroscopy (ARPES). We uncover coexisting near *C*₄-distributed and *C*₂-distributed Fermi surfaces. High-resolution measurements at low temperatures reveal no detectable spin-density wave (SDW) gap, which disfavors an SDW-driven scenario for the magnetic excitations. Instead, resonant ARPES suggests band-selective Kondo coupling on a subset of small *C*₂-distributed pockets aligned with the Ce ladder, generating intrinsically anisotropic magnetic exchange and competing FM/AFM tendencies. This band-selective magnetic interaction provides a natural microscopic basis for the emergence of q1D ferromagnetic fluctuations in CeSb₂, demonstrating how such coupling can generate q1D spin fluctuations in a q2D system.

High-quality single crystals of CeSb₂ were grown by the self-flux method within a graphite resistance heating system [26]. Samples were cleaved *in-situ* below 30 K along the (001) plane. ARPES measurements were performed at the synchrotron radiation facilities-Advanced Light Source (ALS), Shanghai Synchrotron Radiation Facility (SSRF), and BESSY-II under optimized experimental conditions. More details on sample growth [26] and characterization [22, 24, 25, 27–29], dynamical mean-field theory (DMFT) calculations [30–34], and ARPES measurements were provided in Supplemental Materials (SM) Sections I-IV [35].

The electronic structure of CeSb₂ shows q2D character, as revealed by photon-energy dependent measurements [Fig. S3]. The representative in-plane Fermi surfaces consist of multiple features [Figs. 1(c) and 1(d)]. An inner square-like β pocket and an outer diamond-shaped γ pocket are cen-

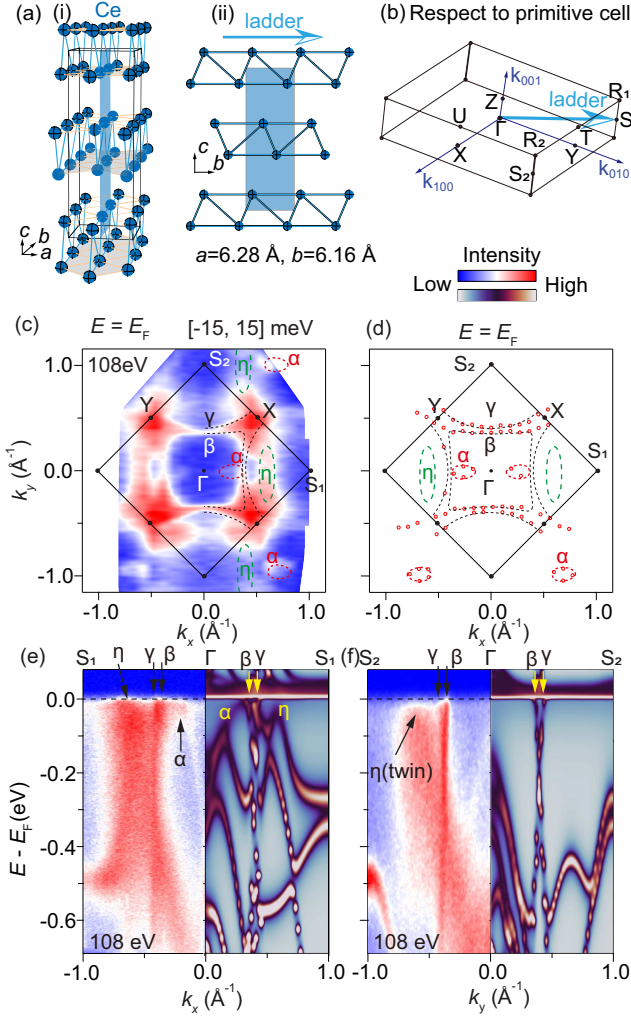


FIG. 1. (a) Crystal structure of CeSb_2 : (i) orthorhombic unit cell with the Ce sublattice highlighted; (ii) with the leg direction along the crystallographic b -axis (blue arrow). (b) Bulk Brillouin zone (BZ) with respect to the primitive cell. The Ce-ladder leg direction (b) corresponds to ΓS_1 . (c) Fermi surface map measured at 6 K with 108 eV LH-polarized photons. (d) Schematic Fermi surfaces derived from (c). (e) and (f) Band dispersions along the ΓS_1 and ΓS_2 directions, together with DMFT calculations.

tered around the Γ point [Figs. 1(c) and 1(d)], both preserving a nearly C_4 symmetry. These two Fermi surfaces cross at the X and Y high-symmetry points in a complex manner according to calculations [Fig. S2] [23]; the details of these crossings are not well resolved in ARPES. In addition, two small α pockets and two small η pockets are primarily located along the ΓS_1 direction [Figs. 1(c)-1(e)], reflecting the quasi-one-dimensional character of the Ce ladder and its intrinsic C_2 symmetrical distribution [Figs. 1(a)-1(b)]. Polarization-dependent measurements show that the C_2 -distributed feature persists under both linear horizontal (LH) and linear vertical (LV) geometries [Fig. S4], ruling out matrix-element effects. Along both ΓS_1 and ΓS_2 [Figs. 1(e) and 1(f)], the β and γ bands are highly dispersive and cross E_F with a relatively large

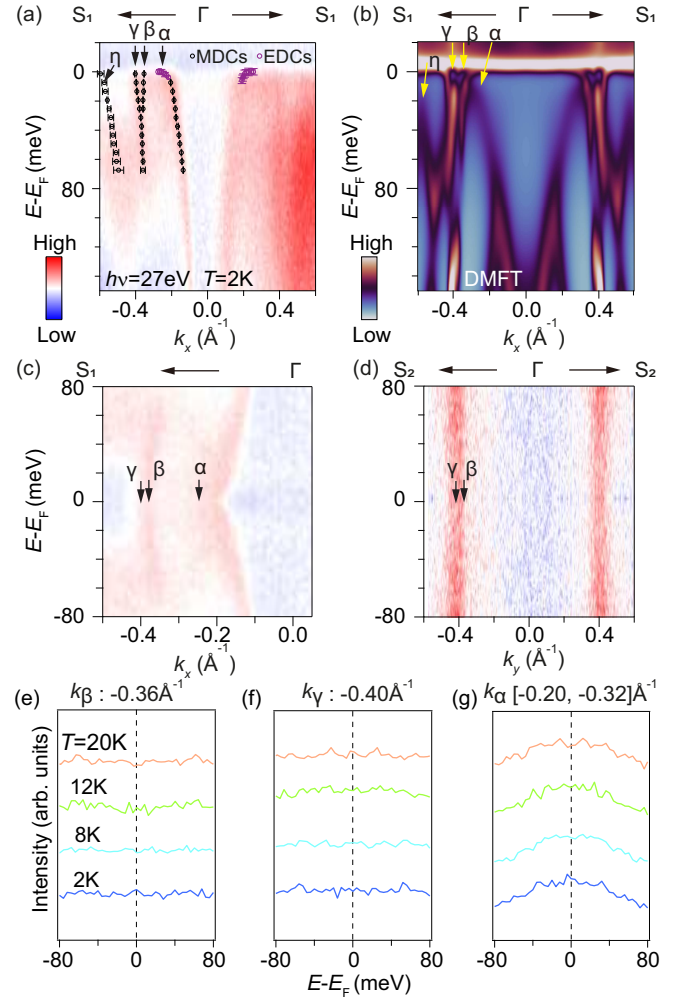


FIG. 2. (a) Valence band dispersions near E_F measured at 2 K with 27 eV photons, corresponding to the $k_z = \pi$ plane. (b) Corresponding band dispersions from DMFT calculations. (c) and (d) Symmetrized energy-momentum (E - k) intensity plots along ΓS_1 (2 K) and ΓS_2 (5 K) directions, respectively, measured with 27 eV photons. (e)-(g) Temperature-dependent symmetric energy distribution curves (EDCs) at k_β , k_γ and k_α along the ΓS_1 direction.

Fermi velocity, indicating relatively weak electronic correlation. In contrast, the α and η bands show broader spectral features [Fig. 1(e)] and reduced velocities near E_F along ΓS_1 [Figs. 2(a) and 2(b)], characteristic of strong correlations, well reproduced by DMFT calculations [Figs. 1(e) and 1(f)]. In the ARPES spectra along ΓS_2 [Fig. 1(f)], the residual weight of the η band originates from the superposition of 90° -rotated structural twin domains [25]. Micro-ARPES measurements on single-domain [Fig. S4] confirm the absence of η pocket along ΓS_2 , supporting its intrinsic C_2 -distributed character.

Given the parallel segments of the β and γ pockets [Fig. 1(d)], a possible Fermi surface nesting condition might give rise to SDW order and contribute to the competing magnetic orders. To test this scenario, high-resolution ARPES measurements were conducted at low temperature down to

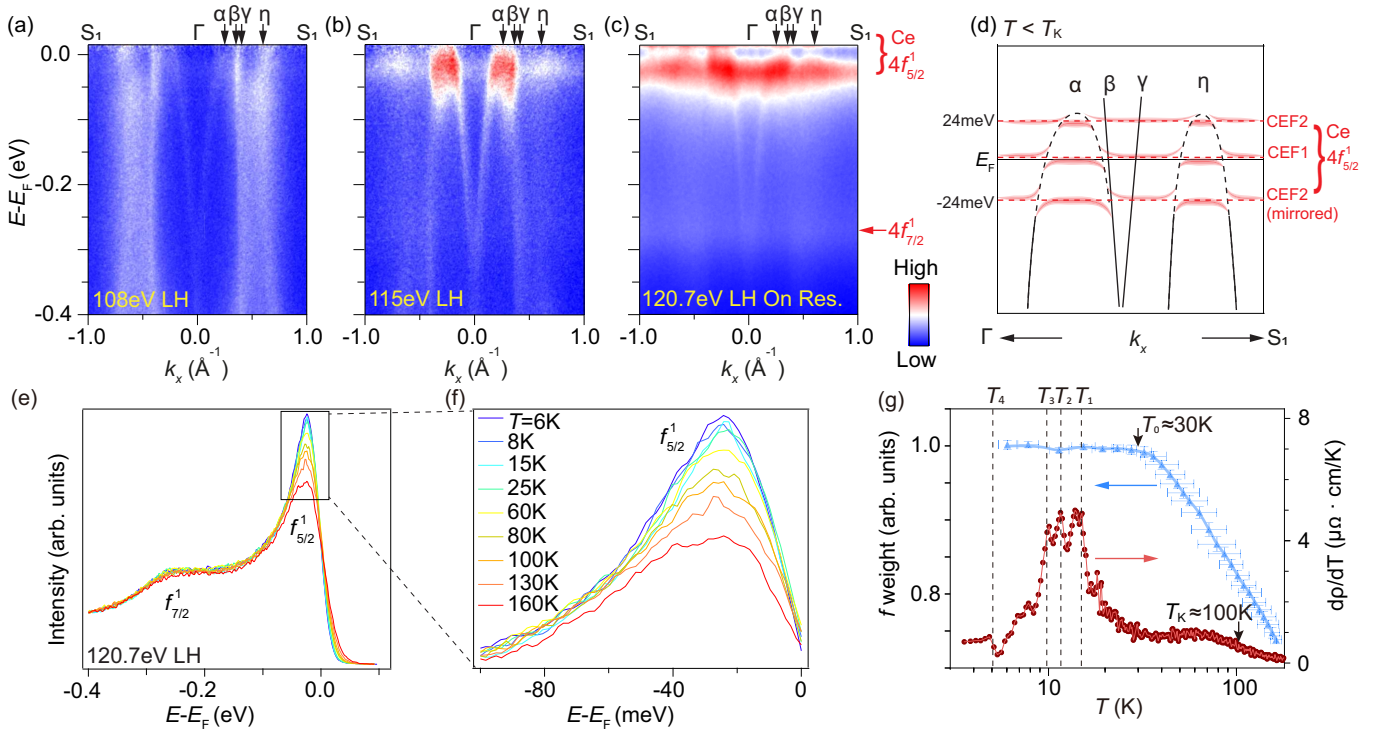


FIG. 3. Photoemission intensity along ΓS_1 direction at 6 K with LH polarized photons at (a) 108 eV (off resonance), (b) 115 eV (pre-edge, partial resonance), and (c) 120.7 eV (on resonance, Ce M -edge), divided by the resolution-convoluted Fermi-Dirac distribution. (d) Schematic of proposed band-selective Kondo coupling with CEF states. (e)-(f) Temperature-dependent EDCs integrated over the momentum range of panel (c). (g) Spectral intensity of $4f_{5/2}^1$ peak over the energy window $[E_F - 0.1 \text{ eV}, E_F + 0.1 \text{ eV}]$, normalized to its value at 6 K. The temperature derivative of resistivity $d\rho/dT$ is plotted to show the T_K and the magnetic transitions.

2 K, yielding a total energy resolution of 3 meV. Symmetrized energy-momentum intensity plots along the ΓS_1 and ΓS_2 directions show no indication of gap opening at the temperature below any ordering transitions, with both β and γ bands dispersing to E_F without suppression of spectral weight. Upon cooling from 20 K to 2 K, the β , γ , and α bands disperse through E_F along ΓS_1 , with no detectable gap across any of the magnetic transitions [Figs. 2(e)-2(g)], within an energy resolution of 3 meV. While we cannot exclude a sub-meV gap or a partial gap, the dominance of well-defined Fermi crossings disfavors nesting as the primary driver of the complex magnetic orders below 16 K.

Resonant ARPES measurements were performed along the ΓS_1 (Ce-ladder) direction by tuning the photon energy across the Ce M -edge. Off-resonance spectra resolve the dispersive α , β , γ and η bands crossing E_F with no observable hybridization gap [Fig. 3(a)]. Upon approaching resonance [Fig. 3(b)] and at resonance [Fig. 3(c)], the spectral weight of Ce $4f$ -derived states is strongly enhanced. Distinct flat features emerge near E_F and at binding energy of ~ 270 meV, which are attributed to the Ce $4f_{5/2}^1$ and $4f_{7/2}^1$ states, respectively. The position of the $4f_{5/2}^1$ feature ~ 24 meV below E_F , differs from that in typical Ce-based heavy-fermion systems such as CeCoIn₅, where the analogous feature lies ~ 2 meV above E_F [36]. It is instead reminiscent of CeSb, where the Ce $4f$ fea-

ture appears ~ 50 meV below E_F , and has been interpreted as a mirrored crystal electric field (CEF) excitation [37]. One possible interpretation of CeSb₂, analogous to CeSb, is illustrated in Fig. 3(d): the primary Ce $4f$ level (CEF1) lies at E_F , accompanied by a CEF excitation at ~ 24 meV above E_F (CEF2) and its mirrored counterpart below E_F . (Independent confirmation of the CEF level from INS and specific heat in CeSb₂ is currently lacking.) In the ARPES spectra, no hybridization gap is resolved at 24 meV for any of the dispersive bands [Figs. 3(a)-3(c)], indicating that hybridization with the CEF2 state is relatively weak. The resonant enhancement is most pronounced for the hole-like α and η bands [Figs. 3(b)-3(c)], indicating band-selective Kondo hybridization/coherence and suggesting that Kondo coupling at E_F with the CEF1 state is finite and occurs on the Ce-ladder-aligned C_2 -distributed Fermi pockets.

The $4f_{5/2}^1$ peak intensity grows monotonically upon cooling [Figs. 3(e) and 3(f)], reflecting the buildup of Kondo coherence. The flat band feature persists up to 160 K [see also Fig. S5], indicating that heavy-quasiparticle formation develops well above the coherence temperature ($T_K \sim 100$ K), as commonly seen in Ce-based heavy-fermion systems [36, 38–41]. The $4f_{5/2}^1$ weight follows a typical Kondo coherence evolution above $T_0 \sim 30$ K but saturates below T_0 [Fig. 3(g)]. The sizable residual moment of $\sim 1.4 \mu_B/\text{Ce}$ at 2 K [25], approaching the free Ce³⁺ Hund's-rule value ($2.54 \mu_B$) and exceeding

that of most Ce-based heavy fermions [42–45], indicates incomplete Kondo screening and the persistence of substantial $4f$ local-moment character on the Ce sites at low temperature. This relocalization-like behavior, similar to that reported in several other Ce-based heavy fermions [46–50], allows partial Kondo coherence to coexist with magnetic order.

The band-selective Kondo coupling has direct consequences for the momentum-space structure of the effective magnetic susceptibility. The resonance-enhanced Fermi surface map highlights the momentum-space distribution of Ce $4f$ spectral weight [Fig. 4(a)]. Besides a generally enhanced intensity in the first Brillouin zone with no obvious correspondence with Fermi surfaces, the α and η pockets exhibit clear band-specific enhancement as also observed in Figs. 3(b)–3(c). Since these pockets are intrinsically C_2 -distributed, appearing along the Ce-ladder direction (b -axis) and absent along ΓS_2 [Figs. 1(c)–(f), Fig. S4], the enhanced Kondo coupling is geometrically confined to the ladder-aligned subset of the Fermi surface. The enhanced Kondo-derived spectral weight at the Fermi wave vectors (k_F) of the α and η pockets [Figs. 4(a)–4(b)] naturally gives rise to a larger effective exchange constant between the itinerant electrons and the residual Ce $4f$ local moments at these momenta. This band-selective anisotropy provides a direct electronic basis for highly anisotropic magnetic exchange parameters, as observed by INS [21]. Specifically, the intra-ladder exchange J_{\parallel} dominates over the inter-ladder coupling J_{\perp} as illustrated in Fig. 4(c), despite the quasi-2D crystal structure.

One plausible manifestation of the band-selective Kondo coupling could be Ruderman-Kittel-Kasuya-Yosida (RKKY)-type magnetic exchange $J(r)$ along the Ce-ladder direction b . Through a simplified simulation in Supplementary Materials Sec. IX [35, 51–53], the α and η pockets favor AFM and FM nearest-neighbor exchange channels, respectively, suggesting competing magnetic interactions and the origin of q1D FM interactions. More intriguingly, within the experimental uncertainty on k_{α} , the contributions from α and η pockets can also produce a significant AFM channel at the third-nearest neighbor, consistent with the experimentally observed commensurate AFM order with propagation vectors $(-1, \pm\frac{1}{6}, 0)$ [21, 25]. These coexisting FM and AFM tendencies provide an electronic mechanism for both the dominant FM excitations and the complex magnetic phase diagram of CeSb₂ that cannot be accounted for by a single FM exchange alone [21].

The f -electron spectral weight saturates below $T_0 \sim 30$ K, indicating incomplete Kondo screening, leaving residual Ce $4f$ moments that remain available for magnetic ordering. The small size of the α and η Fermi pockets suggests a low density of itinerant carriers, which may partially contribute to the incomplete screening of the Ce $4f$ moments. In addition, CEF effects further reduce the f -electron spectral weight near E_F . The combined effect may account for the relatively small effective mass observed in CeSb₂ [29, 54]. Notably, the saturation of f -electron spectral weight occurs above the highest magnetic transition temperature T_1 (~ 15 K) [Fig. 3(e)], suggesting the presence of short-range magnetic correlations that

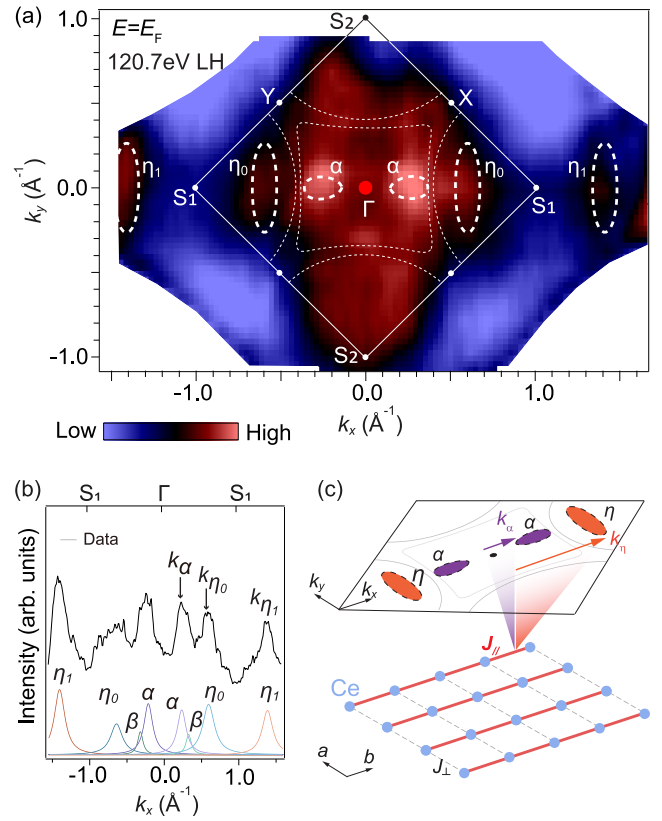


FIG. 4. (a) Fermi surface map in the k_x – k_y plane obtained by resonance-enhanced ARPES at 20 K with $h\nu=120.7$ eV (Ce M-edge), integrated over $[E_F - 25$ meV, $E_F + 25$ meV]. (b) MDC along the ΓS_1 direction at E_F ; The extracted Fermi wavevectors are estimated from the Lorentzian peak positions [Table II in Ref. [35]]. (c) Schematic of the proposed band-selective Kondo coupling mechanism and resulting exchange anisotropy.

persist into the paramagnetic regime. This is consistent with neutron scattering results showing well-defined q1D paramagnons [21]. The coexistence of band-selective Kondo coherence and persistent spin fluctuations in the paramagnetic regime may be relevant to the emergence of pressure-induced superconductivity [9, 55–57].

In summary, we have identified band-selective Kondo coupling as a microscopic electronic mechanism underlying the q1D FM excitations in CeSb₂. The selective hybridization between Ce $4f$ local moments and the C_2 -distributed Fermi pockets aligned with the Ce ladder gives rise to anisotropic Kondo-mediated exchange interactions. Unlike conventional RKKY scenarios in which all conduction-electron pockets contribute uniformly to the exchange, our results reveal a band-selective mechanism in which only the ladder-aligned, Kondo-coupled pockets dominate the magnetic interactions. More broadly, our results suggest that band-selective Kondo coupling can effectively reduce the dimensionality of magnetic interactions independently of the underlying crystal lattice, providing a general electronic route to emergent q1D magnetism in correlated f -electron systems.

Acknowledgments – We gratefully acknowledge the valuable discussion with Guangming Zhang, Liyang Qiu and Michael Smidman. We also thank the experimental support of Chris Jozwiak, Emile Rienks, ZhiCheng Jiang, Yichen Yang, Zhengtai Liu, Gexing Qu and Zhenhua Chen. This work is supported in part by the National Science Foundation of China under the grant Nos. 12422404, 92477206, 12274085, 92365302, the National Key R&D Program of the MOST of China (2023YFA1406300), the New Cornerstone Science Foundation, the Quantum Science and Technology-National Science and Technology Major Project (Grant No.2021ZD0302803), and Shanghai Municipal Science and Technology Major Project (Grant No.2019SHZDZX01). Yifei Fang acknowledges CAS Project for Young Scientists in Basic Research (YSBR-127). The use of the Advanced Light Source, BL7.0.2, is supported by the U.S. Department of Energy, Office of Science, Office of Basic Energy Sciences under Contract No.DE-AC02-76SF00515. The low temperature and high resolution ARPES measurements were carried out at the One-cubed ARPES end-station at the BESSY II electron storage ring operated by the Helmholtz-Zentrum Berlin für Materialien und Energie. Part of this research used Beamline 03U (<https://cstr.cn/31124.02.SSRF.BL03U>) of the Shanghai Synchrotron Radiation Facility. Some preliminary data were taken at BL09U (<https://cstr.cn/31124.02.SSRF.BL09U>) of the Shanghai Synchrotron Radiation Facility.

* pengrui@fudan.edu.cn

† xuhaichao@fudan.edu.cn

- [1] K. Miyake, S. Schmitt-Rink, and C. Varma, *Physical Review B* **34**, 6554 (1986).
- [2] M. Fujita, H. Hiraka, M. Matsuda, M. Matsuura, J. M. Tranquada, S. Wakimoto, G. Xu, and K. Yamada, *Journal of the Physical Society of Japan* **81**, 011007 (2011).
- [3] D. J. Scalapino, *Reviews of Modern Physics* **84**, 1383 (2012).
- [4] M. Dean, A. James, R. Springell, X. Liu, C. Monney, K. Zhou, R. Konik, J. Wen, Z. Xu, G. Gu, *et al.*, *Physical Review Letters* **110**, 147001 (2013).
- [5] H. Zhi, T. Imai, F. Ning, J.-K. Bao, and G.-H. Cao, *Physical Review Letters* **114**, 147004 (2015).
- [6] J.-K. Bao, J.-Y. Liu, C.-W. Ma, Z.-H. Meng, Z.-T. Tang, Y.-L. Sun, H.-F. Zhai, H. Jiang, H. Bai, C.-M. Feng, *et al.*, *Physical Review X* **5**, 011013 (2015).
- [7] F. Balakirev, T. Kong, M. Jaime, R. McDonald, C. Mielke, A. Gurevich, P. Canfield, and S. Bud'ko, *Physical Review B* **91**, 220505 (2015).
- [8] J. Yang, J. Luo, C. Yi, Y. Shi, Y. Zhou, and G.-q. Zheng, *Science Advances* **7**, eabl4432 (2021).
- [9] S. Ran, C. Eckberg, Q.-P. Ding, Y. Furukawa, T. Metz, S. R. Saha, I.-L. Liu, M. Zic, H. Kim, J. Paglione, *et al.*, *Science* **365**, 684 (2019).
- [10] Y. Xu, Y. Sheng, and Y.-f. Yang, *Physical Review Letters* **123**, 217002 (2019).
- [11] W. Knafo, G. Knebel, P. Steffens, K. Kaneko, A. Rosuel, J.-P. Brison, J. Flouquet, D. Aoki, G. Lapertot, and S. Raymond, *Physical Review B* **104**, L100409 (2021).
- [12] Y. Li, X. Xu, M.-H. Lee, M.-W. Chu, and C. Chien, *Science* **366**, 238 (2019).
- [13] K. Ishihara, M. Roppongi, M. Kobayashi, K. Imamura, Y. Mizukami, H. Sakai, P. Opletal, Y. Tokiwa, Y. Haga, K. Hashimoto, *et al.*, *Nature Communications* **14**, 2966 (2023).
- [14] Y. Tsutsumi and K. Machida, *Physical Review B* **110**, L060507 (2024).
- [15] X.-X. Wu, C.-C. Le, J. Yuan, H. Fan, and J.-P. Hu, *Chinese Physics Letters* **32**, 057401 (2015).
- [16] G. Cuono, F. Forte, A. Romano, X. Ming, J. Luo, C. Autieri, and C. Noce, *Physical Review B* **103**, 214406 (2021).
- [17] S. Sundar, S. Gheidi, K. Akintola, A. Côté, S. Dunsiger, S. Ran, N. Butch, S. Saha, J. Paglione, and J. Sonier, *Physical Review B* **100**, 140502 (2019).
- [18] C. Duan, K. Sasmal, M. B. Maple, A. Podlesnyak, J.-X. Zhu, Q. Si, and P. Dai, *Physical Review Letters* **125**, 237003 (2020).
- [19] C. Duan, R. Baumbach, A. Podlesnyak, Y. Deng, C. Moir, A. J. Breindel, M. B. Maple, E. Nica, Q. Si, and P. Dai, *Nature* **600**, 636 (2021).
- [20] O. P. Squire, S. A. Hodgson, J. Chen, V. Fedoseev, C. K. de Podesta, T. I. Weinberger, P. L. Alireza, and F. M. Grosche, *Physical Review Letters* **131**, 026001 (2023).
- [21] Z. Shan, Y. Jiao, J. Guo, Y. Wang, J. Wu, J. Zhang, Y. Zhang, D. Su, D. T. Adroja, C. Balz, *et al.*, *Physical Review Letters* **134**, 116704 (2025).
- [22] Y. Zhang, X. Zhu, B. Hu, S. Tan, D. Xie, W. Feng, L. Qin, W. Zhang, Y. Liu, H. Song, *et al.*, *Chinese Physics B* **26**, 067102 (2017).
- [23] Y. Zhang, X. Luo, W. Feng, S. Tan, Q. Hao, Q. Zhang, D. Yuan, B. Wang, Y. Liu, Q. Liu, *et al.*, *Physical Review B* **106**, 045133 (2022).
- [24] C. Trainer, C. Abel, S. L. Bud'ko, P. C. Canfield, and P. Wahl, *Physical Review B* **104**, 205134 (2021).
- [25] B. Liu, L. Wang, I. Radelytskyi, Y. Zhang, M. Meven, H. Deng, F. Zhu, Y. Su, X. Zhu, S. Tan, *et al.*, *Journal of Physics: Condensed Matter* **32**, 405605 (2020).
- [26] S. Zhang, M. Li, Y. Yang, C. Zhao, M. He, Y. Hang, and Y. Fang, *CrystEngComm* **23**, 5045 (2021).
- [27] P. C. Canfield, J. Thompson, and Z. Fisk, *Journal of Applied Physics* **70**, 5992 (1991).
- [28] S. L. Bud'ko, P. Canfield, C. Mielke, and A. Lacerda, *Physical Review B* **57**, 13624 (1998).
- [29] R. F. Luccas, A. Fente, J. Hanko, A. Correa-Orellana, E. Herrera, E. Climent-Pascual, J. Azpeitia, T. Pérez-Castañeda, M. Osorio, E. Salas-Colera, *et al.*, *Physical Review B* **92**, 235153 (2015).
- [30] K. Haule, C.-H. Yee, and K. Kim, *Physical Review B* **81**, 195107 (2010).
- [31] K. Haule and T. Birol, *Physical Review Letters* **115**, 256402 (2015).
- [32] P. Blaha, K. Schwarz, F. Tran, R. Laskowski, G. K. Madsen, and L. D. Marks, *The Journal of Chemical Physics* **152**, 074101 (2020).
- [33] K. Haule, *Physical Review Letters* **115**, 196403 (2015).
- [34] E. Gull, A. J. Millis, A. I. Lichtenstein, A. N. Rubtsov, M. Troyer, and P. Werner, *Reviews of Modern Physics* **83**, 349 (2011).
- [35] See Supplemental Material.
- [36] Q. Chen, D. Xu, X. Niu, J. Jiang, R. Peng, H. Xu, C. Wen, Z. Ding, K. Huang, L. Shu, *et al.*, *Physical Review B* **96**, 045107 (2017).
- [37] S. Jang, R. Kealhofer, C. John, S. Doyle, J.-S. Hong, J. H. Shim, Q. Si, O. Erten, J. D. Denlinger, and J. G. Analytis, *Science Advances* **5**, eaat7158 (2019).
- [38] Q. Chen, D. Xu, X. Niu, R. Peng, H. C. Xu, C. Wen, X. Liu,

- L. Shu, S. Tan, X. Lai, *et al.*, *Physical Review Letters* **120**, 066403 (2018).
- [39] Q. Chen, C. Wen, Q. Yao, K. Huang, Z. Ding, L. Shu, X. Niu, Y. Zhang, X. Lai, Y. Huang, *et al.*, *Physical Review B* **97**, 075149 (2018).
- [40] G. Poelchen, S. Schulz, M. Mende, M. Güttler, A. Generalov, A. V. Fedorov, N. Caroca-Canales, C. Geibel, K. Kliemt, C. Krellner, *et al.*, *npj Quantum Materials* **5**, 70 (2020).
- [41] Z. Wu, Y. Fang, H. Su, W. Xie, P. Li, Y. Wu, Y. Huang, D. Shen, B. Thiagarajan, J. Adell, *et al.*, *Physical Review Letters* **127**, 067002 (2021).
- [42] G. Knopp, A. Loidl, K. Knorr, L. Pawlak, M. Duczmal, R. Caspary, U. Gottwick, H. Spille, F. Steglich, and A. Murani, *Zeitschrift für Physik B Condensed Matter* **77**, 95 (1989).
- [43] D. M. Fobes, E. D. Bauer, J. D. Thompson, A. Sazonov, V. Hutanu, S. Zhang, F. Ronning, and M. Janoschek, *Journal of Physics: Condensed Matter* **29**, 17LT01 (2017).
- [44] M. Raba, E. Ressouche, N. Qureshi, C. Colin, V. Nassif, S. Ota, Y. Hirose, R. Settai, P. Rodière, and I. Sheikin, *Physical Review B* **95**, 161102 (2017).
- [45] M. Smidman, D. Adroja, A. D. Hillier, L. Chapon, J. Taylor, V. Anand, R. P. Singh, M. R. Lees, E. Goremychkin, M. Koza, *et al.*, *Physical Review B* **88**, 134416 (2013).
- [46] Y. Luo, C. Zhang, Q.-Y. Wu, F.-Y. Wu, J.-J. Song, W. Xia, Y. Guo, J. Ruzs, P. M. Oppeneer, T. Durakiewicz, *et al.*, *Physical Review B* **101**, 115129 (2020).
- [47] N. apRoberts Warren, A. Dioguardi, A. Shockley, C. Lin, J. Crocker, P. Klavins, D. Pines, Y.-F. Yang, and N. Curro, *Physical Review B* **83**, 060408 (2011).
- [48] K. R. Shirer, A. C. Shockley, A. P. Dioguardi, J. Crocker, C. H. Lin, N. apRoberts Warren, D. M. Nisson, P. Klavins, J. C. Cooley, Y.-f. Yang, *et al.*, *Proceedings of the National Academy of Sciences* **109**, E3067 (2012).
- [49] P. Li, H. Ye, Y. Hu, Y. Fang, Z. Xiao, Z. Wu, Z. Shan, R. P. Singh, G. Balakrishnan, D. Shen, *et al.*, *Physical Review B* **107**, L201104 (2023).
- [50] F.-Y. Wu, Q.-Y. Wu, C. Zhang, Y. Luo, X. Liu, Y.-F. Xu, D.-H. Lu, M. Hashimoto, H. Liu, Y.-Z. Zhao, *et al.*, *Frontiers of Physics* **18**, 53304 (2023).
- [51] V. Litvinov and V. Dugaev, *Physical Review B* **58**, 3584 (1998).
- [52] S. Blundell, *Magnetism in condensed matter* (OUP Oxford, 2001).
- [53] T. M. Rusin and W. Zawadzki, *Journal of Magnetism and Magnetic Materials* **441**, 387 (2017).
- [54] B. K. Gamble, *Specific heat and transport properties of the light rare-earth dioxides* (Clemson University, 2002).
- [55] J. Arndt, O. Stockert, K. Schmalzl, E. Faulhaber, H. S. Jeevan, C. Geibel, W. Schmidt, M. Loewenhaupt, and F. Steglich, *Physical Review Letters* **106**, 246401 (2011).
- [56] S. Saxena, P. Agarwal, K. Ahilan, F. Grosche, R. Haselwimmer, M. Steiner, E. Pugh, I. Walker, S. Julian, P. Monthoux, *et al.*, *Nature* **406**, 587 (2000).
- [57] D. Aoki, A. Huxley, E. Ressouche, D. Braithwaite, J. Flouquet, J.-P. Brison, E. Lhotel, and C. Paulsen, *Nature* **413**, 613 (2001).